RECONSTRUCTING IVUS IMAGES FOR AN ACCURATE TISSUE CLASSIFICATION

Karla L Caballero, Joel Barajas
Computer Vision Center, Autonomous University of Barcelona, Edificio O Campus UAB, Bellaterra, Spain

Oriol Pujol
Dept. Matemàtica Aplicada i Anàlisi. University of Barcelona, Computer Vision Center, Barcelona, Spain

Josefina Mauri
Hospital Universitari German Trias i Pujol, Badalona, Spain

Petia Radeva
Computer Vision Center, Autonomous University of Barcelona, Bellaterra, Spain

Keywords: Intravascular Ultrasound, RF signals, Image Reconstruction, Tissue Classification, Adaboost, ECOC.

Abstract: Plaque rupture in coronary vessels is one of the principal causes of sudden death in western societies. Reliable diagnostic tools are of great interest for physicians in order to detect and quantify vulnerable plaque in order to develop an effective treatment. To achieve this, a tissue classification must be performed. Intravascular Ultrasound (IVUS) represents a powerful technique to explore the vessel walls and to observe its morphology and histological properties. In this paper, we propose a method to reconstruct IVUS images from the raw Radio Frequency (RF) data coming from the ultrasound catheter. This framework offers a normalization scheme to compare accurately different patient studies. Then, an automatic tissue classification based on the texture analysis of these images and the use of Adapting Boosting (AdaBoost) learning technique combined with Error Correcting Output Codes (ECOC) is presented. In this study, 9 *in-vivo* cases are reconstructed with 7 different parameter set. This method improves the classification rate based on images, yielding a 91% of well-detected tissue using the best parameter set. It is also reduced the inter-patient variability compared with the analysis of DICOM images, which are obtained from the commercial equipment.

1 INTRODUCTION

Nowadays cardiovascular diseases are one of the principal causes of sudden death in the western societies. In particular, acute coronary syndrome is caused by plaque rupture in coronary vessels. Therefore, an accurate preventive detection and quantification of this vulnerable plaque is of great relevance for the medical community.

Intravascular Ultrasound (IVUS) Imaging is an image modality based on the ultrasound reflection from the vessel wall. In this kind of study, a catheter composed of a radio frequency (RF) emitter and a transducer is introduced into the coronaries to perform an exploration. Here, RF beams are distributed around the vessel and the transducer collects their reflections yielding a descriptive cross-sectional image of the vessel. There are three distinguishable plaques: calcified tissue (characterized by a very high echo-reflectivity and absorbtion), fibrous plaque (medium echo-reflectivity and good transmission coefficient), and lipidic or soft plaque (very low reflectance). Based on IVUS images, the automatic analysis of these tissues represents a feasible way to predict and quantify the vulnerable plaques, avoiding the subjectivity due to the high inter-observer variability of these studies.

However the acquisition of normalized DICOM images represents a singular challenge, because each physician can acquire these with a different parametrization. Additionally, once these images are recorded, it becomes very difficult to change their

L Caballero K., Barajas J., Pujol O., Mauri J. and Radeva P. (2007).
RECONSTRUCTING IVUS IMAGES FOR AN ACCURATE TISSUE CLASSIFICATION.
In *Proceedings of the Second International Conference on Computer Vision Theory and Applications*, pages 113-119
DOI: 10.5220/0002061001130119

contrast, since it is equalized radially with a non linear model, and the reconstruction parameters are not longer available. This lack of normalization hinders the automatic classification since the tissues from two different patients may not be comparable due to the difference in appearance.

In this paper, we propose the normalization of the IVUS images by means of reconstructing them from the RF signals coming from the catheter of the IVUS equipment. It gives us the opportunity to normalize different pullbacks to the same parameter set. Moreover, we can choose the reconstruction parameterization that shows the best tissue classification rate in terms of high accuracy and small inter-patient variability.

This paper is organized in the following manner: in section 2 the comparison between the DICOM and reconstructed images is detailed. In section 3 the reconstruction process is explained. The feature extraction using texture descriptors is shown in section 4. Section 5 explains the characterization process. Finally, sections 6 and 7 show the results and conclusion, respectively.

2 IMAGE RECONSTRUCTION PROCESS

An IVUS equipment consists of a main computer to reconstruct images, and a catheter which is introduced into the vessel to perform an exploration. This catheter carries an ultrasound emitter which shots a number of beams radially, and a transducer that collects their reflections as RF signals. Based on the type of tissue, these signals vary their frequency and amplitude. Then, these are processed to build a circular image where the amplitude of the signal is represented in gray scale.

2.1 RF Signal Acquisition

The RF signals have been acquired from a Boston Sci. Galaxy II using a 12-bit Acquiris acquisition card with a sampling rate of $200MHz$. The frequency of the catheter transducer is $40Mhz$ for our data, and it is assumed a sound speed in tissue of $1565m/s$. Each IVUS image consists of a total of 256 A-lines (ultrasound beams), and a length of $4.9mm$. This information was captured from patient pullback sequences *in vivo* consisting typically of 2000 images. Figure 1(a) shows an example of a raw RF A-line.

2.2 Image Construction

Once the RF signals have been acquired, an image construction framework is applied to obtain the IVUS images with a fixed parameter set. As a preprocessing step, the signals are filtered using a butterworth bandpass with 50% of gain centered at the transducer frequency. It is employed to reduce the low frequency noise not coming from the transducer response. Due to the plastic cover of the catheter head, huge low-frequency waves appears at the beginning of every A-line. Since these are signal artifacts, the filter is used to reduce these effects. In figure 1(b) a filtered A-line is displayed. It can be observed that the initial low frequency peaks have been eliminated, and just the transducer response remains. Additionally, in order to correct the attenuation caused by the tissue, an exponential time gain compensation (TGC) is defined as:

$$TGC = 1 - e^{-\beta r}$$
$$\beta = \ln 10^{\alpha f/20}$$

where $\alpha = 1DbMhz/s$ is the attenuation factor of the tissue, and f is the frequency of the transducer. In practice, it is not feasible to apply different factors, one for each tissue, when there is not previous information about the presence of specific plaques. Therefore, a weighted average of the possible factors is used.

After the signals are compensated, their envelope is calculated using the Hilbert transform. Figure 1(c) depicts a compensated A-line along with its envelope. Notice that the tissue reflections have increased their amplitude based on their position. The 256 A-lines, which compose an image, have been arranged into a polar image. In order to distribute the gray levels of its histogram, the envelopes have been normalized in a range from 0 to 1, and compressed in a logarithmical form enhancing its visualization. In figure 1(d) a polar image after compression is shown. Here the *x*-axis represent the different angles and the *y*-axis the depth.

The image is constructed in cartesian form and the missing pixels between each angle are filled using bilinear interpolation. Then, a nonlinear Digital Development Process (DDP) to regulate the contrast radially is applied(Gonzales and Woods, 1992). This step consists in dividing the image radially in several sections, in order to obtain the same equalization used by IVUS equipment. Those sections are normalized and filtered separately according to the interpolation level. Then, a weighted contrast is applied to uniform all the image such that its distribution in the image along the radius is fixed and only one parameter gain is changed.

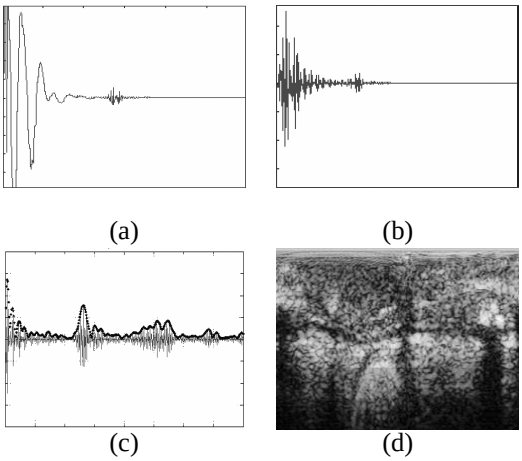

Figure 1: IVUS image reconstruction steps: a)RF signal acquisition of an A-line, b)filtered signal c)envelope calculation from a compensated signal, d)polar image before their cartesian construction.

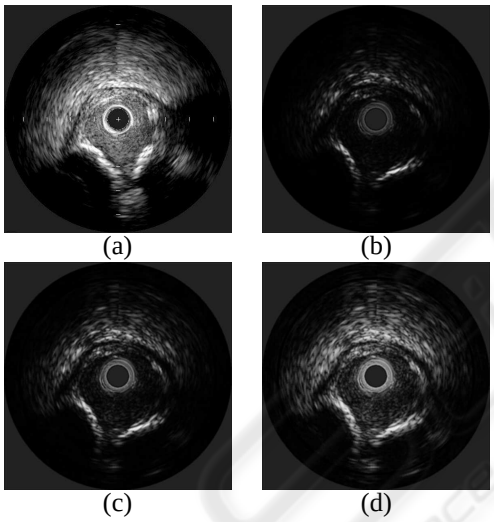

Figure 2: IVUS images and Reconstructed IVUS images from RF signals with different DDP gain parameters. (a)Dicom image from the IVUS equipment.(b)DDP gain parameter fixed to 1.04. (c)DDP gain parameter fixed to 2.20. (d)DDP gain parameter fixed to 3.40.

The parameters are fixed in order to normalize images from different patients. This process allows us to change the gain parameter of the image easily with low computational cost. It is not an easy task in the DICOM images since each pullback can be saved by a different person, and the reconstruction parameters are not usually available. Figure 2.2 shows an example of constructed images with different gains compared with a DICOM image.

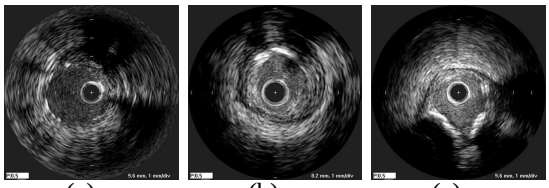

Figure 3: Dicom images from different patients saved with different parameter set.

3 RECONSTRUCTED IMAGE VS DICOM IMAGE

When the IVUS study is performed, DICOM images are generated automatically. Because of its nature, these are recorded at one specific gain or parametrization. However, when a multiple observer study is needed, the images can not been adjusted anymore, since the signal information, the RF signal is lost.

To improve the visualization, DICOM images diminish the visibility of the outer radius in order to increase the focus on the inner regions. This procedure can hinder an automatic classification. It is because a specific tissue can be visualized with different appearance in the inner part than in the outer part, and from patient to patient. Figure 3 shows examples of DICOM images from various patients recorded with different parameter sets. Here it can be visualized an image with the same weight over the entire depth in (a), in (b) the contrast in the inner radius is increased, while in (c) the outer radio is diminished. It suggests a high variability at the time of studying various patients, since the tissue may have not the same gray level and texture properties.

The reconstructed images represent a form of recording all the information of the images. This is achieved by saving the Radio Frequency Signals coming from the IVUS equipment. In this way, images can be reconstructed using different parameterizations without losing any information since any part of the radius can be highlighted to improve the visualization.

4 TEXTURE FEATURES EXTRACTION

In order to perform a tissue characterization, features from the image should be extracted. It has been shown in literature that texture descriptors are robust in presence of noise (P. Ohanian, 1992; Husoy, 1999), as is the case of IVUS images. In this issue, we have

selected three families of general texture descriptors, Co-occurrence matrix measures, Local Binary Patterns and Gabor Filter Banks. Additionally, we have computed the presence of shading as a complementary feature.

4.1 Co-occurrence Matrix

The co-occurrence matrix can be defined as an estimation of the joint probality density function of gray level pairs in a image (P. Ohanian, 1992). The element values in a matrix are bounded from 0 to 1 and the sum of all element values is:

$$P(i,j,D,\theta) = P(I(l,m) = i \otimes I(l+Dcos(\theta), m+Dsin(\theta)) = j),$$

where $I(l,m)$ is the gray value at the pixel(l,m), D is the distance among pixels and θ is the angle of each of neighbors. The angle orientation θ has been fixed to be $[0^o, 45^o, 90^o, 135^o]$, because, according to (Husoy, 1999; P. Ohanian, 1992), it is the minimum set of orientations needed to describe a second-order statistic measures of texture. After computing this matrix, six characterizing measures, energy, entropy, the Inverse Difference Moment, shade, inertia and Promenance are extracted as defined in (P. Ohanian, 1992). Thus, a 48 feature space is built for each pixel, since we are estimating 6 different measures at 4 orientations and two distances $D = [5,8]$.

4.2 Local Binary Patterns

These feature extractor operators are used to detect uniform texture patterns in circular neighborhoods with any quantization of angular space and spatial resolution (Ojala and Maenpaa, 2002). They are based on a circular symmetric neighborhood of P members of a circle with radius R. Gray level invariance is achieved when the central pixel g_c is subtracted to each neighbor g_p, assigning to the result 1 if the difference is positive and 0 if it is negative. Each neighbor is weighted with a 2^p value. Then, the neighbors are added, and the result is assigned to the central pixel.

$$LBP_{R,P} = \sum_{p=0}^{P} s(g_p - g_c) \cdot 2^p$$

With these operators we generate a 3 dimensional space, by applying a radius of $R = [1,2,3]$ and a neighborhood of $P = [8,16,24]$.

4.3 Gabor Filters Bank

The Gabor Filters is an special case of wavelets (Daugman, 1985; Feichtinger and Strohmer, 1998). It is a Gaussian g modulated by a complex sinusoid s. In 2D, a Gabor filter has the following form in the spatial domain:

$$h(x,y) = \frac{1}{2\pi\sigma_{x'}\sigma_{y'}} \exp\{-\tfrac{1}{2}[(\tfrac{x'}{\sigma_{x'}})^2 + (\tfrac{y'}{\sigma_{y'}})^2]\} \cdot s(x,y),$$

where $s(x,y)$ and the Gaussian rotation are defined as:

$$s(x,y) = \exp[-i2\pi(Ux+Vy)]$$
$$x' = x\cos\theta + y\sin\theta, \quad y' = -x\sin\theta + y\cos\theta.$$

x' and y' represent the spatial coordinates rotated by an angle θ. $\sigma_{x'}$ and $\sigma_{y'}$ are the standard deviations for the Gaussian envelope. An aspect ratio λ and its orientation are defined as:

$$\lambda = \frac{\sigma_{x'}}{\sigma_{y'}}, \quad \phi = \arctan V/U$$

where U and V represent the 2D frequencies of the complex sinusoid.

λ has been fixed to 1 in order to create isotropic gaussian envelopes, that is, both $\sigma_{x'}$ and $\sigma_{y'}$ are equal, and θ is discarded, $\theta = 0$. The 2D frequency, (U,V) have been changed to its polar representation F, ϕ. Thus, we have created a filter bank using the following parameters:

$\sigma_x = \sigma_y = [12.7205, 6.3602, 3.1801, 1.5901]$,
$\phi = [0^o, 45^o, 90^o, 135^o]$,
$F = [0.0442, 0.0884, 0.1768, 0.3536]$,
yielding a 16 dimensional space for each pixel.

4.4 Shading

According to (Gil et al., 2006), one of the main differences in the calcified tissue is the shadow which is appreciated behind it. In order to detect this shadow, we have performed an accumulative mean on a polar image. This measure is performed by calculating the mean, from one pixel to the end of the column. Before that, we have chosen a threshold to give the same weight to the tissue and a smaller one to the shadows. This differs from (Gil et al., 2006), since they want to achieve a rough classification. This operation generates one value for each pixel.

As a result of feature extraction process, we obtain a vector of 68 dimensions for each pixel, which will be used to train the classifier. The main goal of this is to extract the best of each technique in order to improve the classification performance.

5 CLASSIFICATION

Once we have reconstructed and characterized the image, we proceed to the classification in order to identify the different types of plaque. We have established 3 classes of tissue: fibrotic plaque, lipid or

Table 1: ECOC code map used in the classification.

Classes	Classifiers		
	1	2	3
Calcium	1	1	0
Fibrotic Plaque	-1	0	1
Soft Plaque	0	-1	-1

soft plaque, and calcified tissue. We use the Adaptive Boosting (Adaboost) with decision stumps as supervised learning technique.

Adaboost allows us to add ”weak” classifiers until some desired training error is obtained (Viola and Jones, 2001; Schapire, 2001). In each step of the algorithm a feature is chosen and assigned a certain weight, which means how accurate this feature can classify the training data. As a result a linear combination of weak classifiers and weights is obtained.

Since this method is generally used in order to classify 2 classes and we have a multiclass problem, we need to establish a criterium for the different classifiers output. This is achieved by means of Error Correction Output Codes (ECOC) (Pujol et al., 2006). They consist of assigning a code map table which relates classifiers outputs and classes. Then, the final classification is obtained finding the minimum distance between the resulting code and each class codeword.

The ECOC classification map is shown in table 1. Here, the number 0 indicate that the class is not used in the selected classifier. Because there are only two classes left for each classifier, we apply one class versus the other, and not one versus the rest. The 1’s indicate that the classifier should output a positive value when this class is found, and a negative one (-1) when it is not.

Once the three classifiers results are obtained, the Euclidean distance is found between each sample of the test and all the class codes. Thus, the class with the minimum codeword distance to the sample code is assigned.

6 RESULTS

We have reconstructed IVUS images from a set of 9 patients with all the three kinds of plaque. Each patient may have 1 or 2 vessel studies or pullbacks. Then, for each one, 10 to 15 different vessel sections or images are selected to be analyzed.

The experiment has been repeated nine times by picking one patient for testing and the rest for training at each iteration. This is done in order to avoid any possible bias resulting of testing the system with the same information as in the training set. In addition, this gives us a roughly idea of how the classification could behave with new unseen patients.

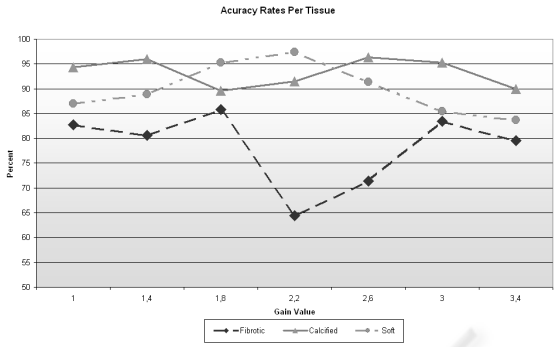

Figure 4: Classification accuracy for each type of tissue among the different DDP gain parameters.

6.1 Tissue Segmentation

We have developed an application to construct IVUS images from the RF signals. This has the advantage of allowing the physicians to chose the parameters of the reconstructed image to simplify the manual segmentation task, since it permits the offline manipulation of the images for the physicians. Although the main purpose of this step is to segment the training data and label it, the parameters used for the segmentation are stored for future analysis yielding to settings normalization.

The physicians have segmented from the vessel images, 50 sections of interests per patient. These segmentations were taken as regions of interest (ROI) which were collected into a database categorized by patient. These were mapped in the reconstructed images in order to construct the data set.

6.2 Classification

The performance of the classification approach was tested by selecting 7 different DDP gain parameters to reconstruct the images. Therefore, 7 different data sets have been created, and their features extracted have been processed separately. For each DDP gain parameter value, a classification error rate has been calculated for every type of tissue.

The accuracy for a range of DDP gain parameters is shown in figure 4. Here it can be observed that the fibrotic plaque is the most difficult to classify compared with the other plaque types. In addition, it is shown that the best accuracy in the 3 plaques

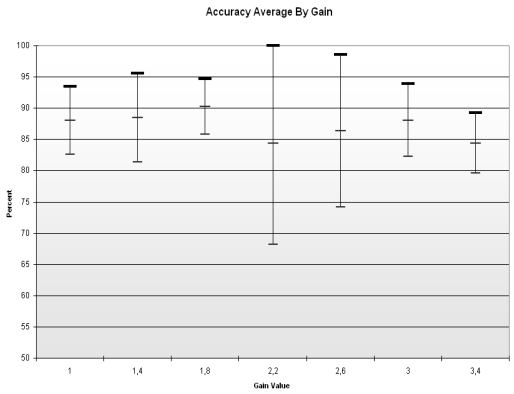

Figure 5: Global classification result among different DDP gain parameters, with their confidence interval.

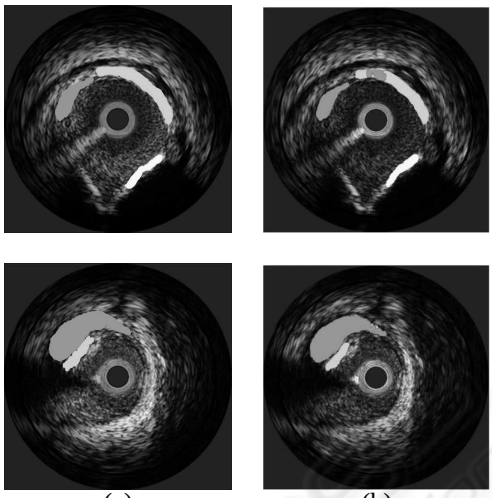

(a) (b)

Figure 6: Image classification result a)Image segmented by the physician, b)Classification Result using the best gain where white is calcified tissue, light gray fibrotic tissue and dark gray lipid tissue.

is achieved when the gain parameter is 1.8, although there are other parameters which have better classification accuracy for an specific plaque.

Additionally, the global accuracy and its confidence interval at 90% for each gain parameter value is calculated using all the patients. This is shown in figure 5. In this picture we can observe that the best classification accuracy is achieved when the gain is equal to 1.8. This value offers us the highest average hit rate and the smallest variability among different patients. Note that with the gain equal to 2.2 give us a similar accuracy rate, but the variability among the different patients is highly significant, which can hinder the classification result with a unseen patient.

In any case, the accuracy rates presented here represents an improvement in the tissue characterization problem with respect to the DICOM based approaches. In this way, we can see that the reconstruction process is a critical step for classification purposes. Usually, the classifications rates reported in DICOM approaches are around of 76% of the overall performance without any kind of postprocessing(Pujol, 2004). The difference is because of the proposed normalization procedure of the data to test our classification framework. Figure 6 shows the result of the automatic classification using the best gain obtained. Here it can be seen that the classification result compared with the physician's segmentation is almost the same.

7 DISCUSSION AND CONCLUSION

A method for tissue classification using IVUS reconstructed images from raw RF data has been presented. The information used in this experiment has been obtained from *in vivo* studies. To reduce the high variability among patients, it has been proposed a normalization scheme where every image is reconstructed with a fixed parameter set. It has been shown that DICOM images can not be normalized easily undermining the classification. On the other hand, by collecting the raw RF information and reconstructing the corresponding images, it is possible to establish a comparative framework which reduces the inter-patient variability.

We have depicted an application of a multi-class problem as a combination of two-class classifiers based on discrete Adaboost using ECOC. It diminishes the ambiguity in classification when tides are found. In addition, the use of this technique simplifies this multi-class issue by reducing the amount of data and the time of training.

It has been performed an statistical analysis to obtain the best reconstruction parameters for classification. Several values of DDP gain parameters have been tested and their hit rate calculated to determine which best improves the plaque classification. In addition, it has been found that the accuracy of classifying reconstructed images is higher than the previously reported using DICOM images.

The use of this framework suggests the possible employment of different gains based on the desired tissue. Here, it can be assigned a different parameter set to classify each plaque, and combine them into a global result.

The classification explained has been performed for each pixel and without any kind of postprocessing. To generalize the response for one tissue in the image, some grouping techniques could be applied. Additionally, by performing these, a mixed plaque composed of small amounts from different tissues, can be defined. This has not been established at class level, since the mixed plaque is a combination of the 3 principal plaques presented.

ACKNOWLEDGEMENTS

This work was supported in part by a research grant from projects TIN2006-15308-C02, FIS-PI061290, by the Generalitat of Catalunya under the FI grant and by the Spanish Ministry of Education and Sciences (MEC) under the FPU grant Ref: AP2005-0926

REFERENCES

Daugman, J. (1985). Uncertainty relation for resolution in space, spatial frequency, and orientation optimized by two-dimensional visual cortical filters. *Journal of the Optical Society of America*, 2(A):1160–1169.

Feichtinger, H. G. and Strohmer, T., editors (1998). *Gabor Analysis and Algorithms: Theory and Applications*. Birkhäuser.

Gil, D., Hernandez, A., Rodrguez, O., Mauri, F., and Radeva, P. (2006). Statistical strategy for anisotropic adventitia modelling in ivus. *IEEE Trans. Medical Imaging*, 27:1022–1030.

Gonzales, R. and Woods, R. (1992). *Image Processing*. Adison - Wesley.

Husoy, T. R. J. H. (1999). Filtering for texture classification: A comparative study. *IEEE Transactions on Pattern Analysis and Machine Intelligence*, 4:291–310.

Ojala, T. and Maenpaa, M. P. T. (2002). Multiresolution gray-scale and rotation invariant texture classification with local binary patterns. *IEEE Transactions on Pattern Analysis and Machine Intelligence*, 24:971–987.

P. Ohanian, R. D. (1992). Performance evaluation for four classes of textural features. *Pattern Recognition*, 25:819–833.

Pujol, O. (2004). *A semi-supervised Statistical Framework and Generative Snakes for IVUS Analysis*. Graficas Rey.

Pujol, O., Radeva, P., and Vitria, J. (2006). Discriminant ecoc: A heuristic method for application dependent design of error correcting output codes. *IEEE Transactions on Pattern Analysis and Machine Intelligence*, 28:1001–1007.

Schapire, R. (2001). The boosting approach to machine learning: An overview.

Viola, P. and Jones, M. (2001). Robust real-time object detection. In *CVPR01*, volume 1, page 511.